Cell-Penetrating Peptide Enhanced Intracellular Raman Imaging and Photodynamic Therapy

ARTICLE *in* MOLECULAR PHARMACEUTICS · MAY 2013

Impact Factor: 4.38 · DOI: 10.1021/mp300634b · Source: PubMed

3 AUTHORS, INCLUDING:

Andrew Fales
Duke University
38 PUBLICATIONS **501** CITATIONS

SEE PROFILE

molecular pharmaceutics

Article

pubs.acs.org/molecularpharmaceutics

Cell-Penetrating Peptide Enhanced Intracellular Raman Imaging and Photodynamic Therapy

Andrew M. Fales,[†,‡] Hsiangkuo Yuan,[†,‡] and Tuan Vo-Dinh*[,†,‡,§]

[†]Fitzpatrick Institute for Photonics, [‡]Department of Biomedical Engineering, and [§]Department of Chemistry, Duke University, Durham, North Carolina 27708, United States

Supporting Information

ABSTRACT: We present the application of a theranostic system combining Raman imaging and the photodynamic therapy (PDT) effect. The theranostic nanoplatform was created by loading the photosensitizer, protoporphyrin IX, onto a Raman-labeled gold nanostar. A cell-penetrating peptide, TAT, enhanced intracellular accumulation of the nanoparticles in order to improve their delivery and efficacy. The plasmonic gold nanostar platform was designed to increase the Raman signal via the surface-enhanced resonance Raman scattering (SERRS) effect. Theranostic SERS imaging and photodynamic therapy using this construct were demonstrated on BT-549 breast cancer cells. The TAT peptide allowed for effective Raman imaging and photosensitization with the nanoparticle construct after a 1 h incubation period. In the absence of the TAT peptide, nanoparticle accumulation in the cells was not sufficient to be observed by Raman imaging or to produce any photosensitization effect after this short incubation period. There was no cytotoxic effect observed after nanoparticle incubation, prior to light activation of the photosensitizer. This report shows the first application of combined SERS imaging and photosensitization from a theranostic nanoparticle construct.

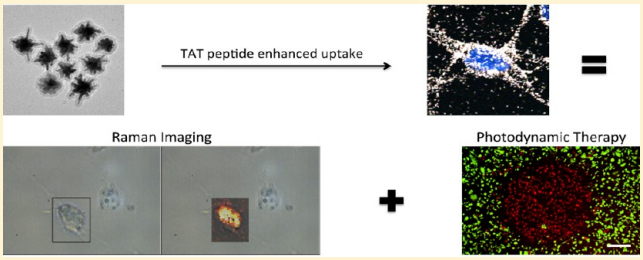

KEYWORDS: *SERS, silica-coated gold nanostar, theranostics, photodynamic therapy, Raman imaging, protoporphyrin IX, cancer*

1. INTRODUCTION

The combination of therapeutic and diagnostic components into a single construct, that is, theranostics, is an emerging field of medical research that aims at further improving personalized medicine.[1−5] Such composite materials allow for the imaging and detection of a specific target, monitoring biological and therapeutic processes, followed by localized release of therapeutic agents. In this way, theranostics can greatly improve the specificity and selectivity of various treatments, increasing efficacy while reducing unwanted side effects. Recently, we have developed plasmonic nanoprobes for various photon-triggered therapeutics, including photothermal and photodynamic therapies.[6−9] Our previous work on theranostic nanoplatforms was a proof-of-concept that focused on the synthesis and characterization of the particles. Herein, we show the application of such a construct for Raman imaging and photodynamic therapy, with an enhanced therapeutic efficacy when using the cell-penetrating TAT peptide.

For the last three decades, our laboratory has been involved in the development and application of a wide variety of plasmonic platforms ranging form nanoparticles to nanowaves, nanoposts, nanowires, and nanochips for use with surface-enhanced Raman scattering (SERS).[10−13] In recent years, Raman-labeled nanoparticle probes have been gaining increasing interest in biolabeling applications due to their advantages over conventional fluorescence methods.[14−30] Fluorophores are highly susceptible to photobleaching, and solvent effects heavily influence fluorescence emission. Multiplex detection with fluorescence is also difficult because of the broad, featureless emission peaks and the need for multiple specific excitation wavelengths. SERS spectra are generally unaffected by photobleaching and solvent or environmental effects. The potential for multiplexing is greater with Raman spectra, owing to the narrow fingerprint-like peaks and the need for only one excitation source. The use of a Raman label whose absorption band overlaps with the laser excitation line can provide surface-enhanced resonance Raman scattering (SERRS), further increasing the signal by a few orders of magnitude.[31]

Photodynamic therapy (PDT) is a modality for the treatment of a number of diseases, including cancer. PDT involves the generation of reactive oxygen species (ROS) by a photosensitizer molecule when excited by the appropriate wavelength of light.[32] The generated ROS then reacts with nearby cellular components causing cell death by apoptosis or necrosis.[33] Protoporphyrin IX (PpIX) is a well-known photosensitizer drug for PDT; however, it has limited efficacy when applied directly to the target site due to its aggregation and poor solubility in aqueous environments.[34,35] One way to overcome these problems is to use a nanoparticle carrier to protect and deliver

Received: November 5, 2012
Revised: April 12, 2013
Accepted: April 18, 2013
Published: April 18, 2013

the drug to the target area. Among other delivery vehicles, mesoporous silica nanoparticles have been shown to be highly effective at encapsulating various PDT drugs while still maintaining their efficacy.[33,34,36−40] This can be achieved due to the fact that the drug does not have to be released at the target; diffusion of molecular oxygen to the drug and diffusion of the generated reactive oxygen species to the environment around the nanoparticle are adequate for therapeutic effects. Silica nanoparticles have also been used as a delivery vehicle for hydrophobic anticancer drugs.[41] The drug-loading capability is not limited to pure silica particles but can also be used with many kinds of silica-coated core−shell nanoparticles.[6,42−45] It has previously been shown that a SERS-labeled nanoparticle, such as a gold nanostar, can be coated with a methylene blue (PDT drug)-loaded silica shell.[6] Gold nanostars are a promising nanoplatform for SERS diagnostics since they exhibit tunable plasmon bands in the NIR tissue optical window and have multiple sharp branches acting as "hot-spots" for the SERS effect.[9,46]

To further improve the efficiency of nanoparticle theranostic systems, sufficient delivery to the target cells is critical. One method for increasing intracellular accumulation of nanoparticles involves the use of a cell-penetrating peptide (CPP).[47−52] One of the first CPPs discovered was the transactivator of transcription (TAT) peptide of the human immunodeficiency virus type 1 (HIV-1) viral genome. Conjugation of the TAT peptide to nanoparticles results in enhanced intracellular delivery, primarily through actin-driven lipid raft-mediated macropinocytosis.[7] TAT has also been used in the development of nuclear-penetrating SERS nanoprobes[27] and X-ray activated drugs.[53]

In this paper we present a CPP-conjugated, PpIX-loaded, SERRS-labeled gold nanostar construct for theranostic application. This integrated construct is applied to both Raman diagnostics (imaging) and PDT, demonstrated on BT-549 breast cancer cells. The CPP-enhanced intracellular accumulation of particles allows for SERRS images to be acquired and PDT to be effective after only 1 h of nanoparticle incubation. Without the CPP, there is little to no SERRS signal detected from the cells and no PDT effect observed after 1 h of incubation with particles. The CPP-enhanced nanoparticle uptake was also verified by two-photon luminescence (TPL) imaging. At the particle concentration used, there is no cytotoxic effect observed on the cells after the 1 h incubation period.

2. EXPERIMENTAL SECTION

2.1. Materials. Gold(III) chloride trihydrate ($HAuCl_4 \cdot 3H_2O$), trisodium citrate dihydrate ($C_6H_5O_7Na_3 \cdot 2H_2O$), 1N HCl, L(+)-ascorbic acid (AA), tetraethyl orthosilicate (TEOS), *O*-[2-(3-mercaptopropionyl-amino)ethyl]-*O*′-methylpolyethylene glycol (mPEG-SH, MW 5k), protoporphyrin IX (PpIX), 3,3′-diethylthiadicarbocyanine iodide (DTDC), fluorescein diacetate (FDA), propidium iodide (PI), and a resazurin based Toxicology Assay Kit (TOX8) were purchased from Sigma-Aldrich (St. Louis, MO, USA) at the highest purity grade available. Silver nitrate ($AgNO_3$, 99.995%) was supplied by Alfa Aesar (Ward Hill, MA, USA). Pure-grade ethanol and ammonium hydroxide (NH_4OH, 29.5%) were obtained through VWR (Radnor, PA, USA). Ultrapure water (>18 MΩ cm^{-1}) was used in all preparations. All glassware was cleaned with *aqua regia*, washed with copious amounts of water, and dried prior to use. Cell culture media and supplements, ProLong Gold Antifade Reagent, and Hoescht 33342 were purchased from Invitrogen (Carlsbad, CA). TAT-peptide (residues 49−57, sequence Arg-Lys-Lys-Arg-Arg-Arg-Gln-Arg-Cys-$CONH_2$) was ordered from SynBioSci (Livermore, CA).

2.2. Instrumentation. Raman spectra were recorded on a Renishaw inVia Raman microscope (Gloucestershire, UK), controlled by WiRE 2.0 software, using an 1800 g mm^{-1} grating with 633 nm (8 mW) excitation. Fluorescence emission spectra were collected using an Edinburgh Photonics FLS920 fluorescence spectrometer (Livingston, UK). Transmission electron microscopy (TEM) was performed on a FEI Tecnai G^2 Twin transmission electron microscope (Hillsboro, OR, USA) with an accelerating voltage of 200 kV. Absorption spectra were acquired on a Shimadzu UV-3600 (Columbia, MD). Particle concentrations and size distributions were measured by Nanoparticle Tracking Analysis (NTA) with a NanoSight NS500 (Amesbury, UK). The fluorescence intensity of the Resazurin-based toxicology assay was measured by a FLUOstar Omega plate reader (BMG LABTECH GmbH, Germany). Photodynamic therapy treatment and cell viability imaging were performed on a Zeiss Axiovert 200 M inverted microscope (Thornwood, NY) equipped with an X-Cite Series 120 mercury arc lamp (Lumen Dynamics, Mississauga, ON, Canada). Images were recorded with a Canon EOS Rebel XTi (Tokyo, Japan) mounted to the front port of the microscope. The TPL images were recorded using a commercial multiphoton microscope (Olympus FV1000, Olympus America, Center Valley, PA) with a femtosecond Ti:sapphire laser (Chameleon Vision II, Coherent, Santa Clara, CA) used for excitation.

2.3. Raman-Labeled Nanostar Synthesis. The nanostars were synthesized according to a previously published protocol.[9] A gold seed solution was prepared by bringing 100 mL of 1 mM $HAuCl_4$ to a rolling boil and adding 15 mL of 1% trisodium citrate under vigorous stirring. The solution was kept boiling for 15 min, cooled, filtered with a 0.22 μm nitrocellulose membrane, and stored at 4 °C. Nanostars were grown from the seed by adding 100 μL of the gold seed to a solution containing 10 mL of 0.25 mM $HAuCl_4$ and 10 μL of 1N HCl, followed quickly by simultaneous addition of 100 μL of 1 mM $AgNO_3$ and 50 μL of 0.1 M AA under moderate stirring. Within 10 s the solution turned from light red to a deep blue. The stock concentration of nanoparticles is approximately 0.1 nM, as determined by Nanoparticle Tracking Analysis (NTA).

Freshly synthesized nanostars (10 mL) were conjugated with mPEG-SH (1 μM final concentration) under gentle stirring for 15 min. The PEGylated particles were then centrifuged (3.5k rcf, 15 min) twice at 4 °C to remove excess PEG and redispersed in water. DTDC (0.2 μM final concentration) in ethanol was added to this solution and allowed to stir overnight. The DTDC-tagged particles were centrifuged (3.5k rcf, 15 min) twice at 4 °C to remove excess DTDC and resuspended in water (AuNS-DTDC).

2.4. Encapsulation of Protoporphyrin IX and TAT Conjugation. A modified Stöber method was used for formation of the silica shell.[54] The labeled nanostar solution was centrifuged at 4 °C (3.5k rcf, 15 min) and resuspended in 2 mL of ethanol. Under gentle stirring, the solution of nanostars was added to a 20 mL glass vial containing 2.0 mL of water and 7.0 mL ethanol. Protoporphyrin IX (1 μM final concentration) in ethanol and 180 μL of NH_4OH were added to the mixture. Silica coating was initiated by the addition of 30 μL of 10% TEOS in ethanol, and the reaction was allowed to proceed for

Scheme 1. Schematic Depiction of the Nanocomposite Synthesis

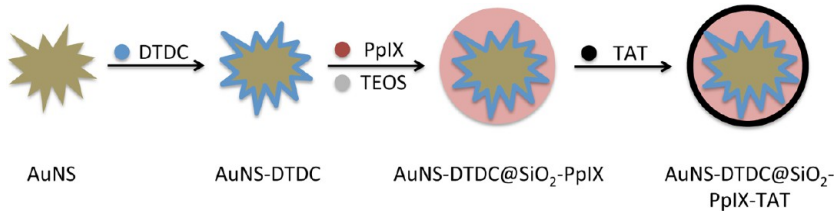

three hours. The nanoparticles were then centrifugally purified (3.5k rcf, 15 min) two times and redispersed into 5 mL of ethanol. TAT conjugation was achieved by passive adsorption; a final concentration of 100 μm TAT was added to the ethanolic solution of particles and allowed to stir overnight.

2.5. Cell Culture and Nanoparticle Incubation. The BT-549 breast cancer cells were a gift from Dr. Victoria Seewaldt. Cells were cultured in modified RPMI 1640 medium (Gibco 22400-089) supplemented with 10% fetal bovine serum and 0.023 IU/mL insulin, and incubated at 37 °C in a humidified 5% CO_2 atmosphere. For PDT studies, cells were seeded into 6-well plates. Cells prepared for Raman mapping were grown on sterilized glass coverslips in 6-well plates. Cytotoxicity was assessed using cells grown in a 96-well plate. Cell samples for two-photon luminescence imaging were grown in 35 mm Petri dishes. All samples were grown to ~80% confluency before use.

The nanoparticle solution was prepared for cellular incubation by centrifugally washing once with water, then resuspending into complete growth medium to a particle concentration of 0.1 nM. Cells were incubated with the particle-containing medium for one hour. After incubation, the medium was aspirated and the cells were washed three times with PBS. For the cytotoxicity assay, growth medium was replaced and the cells were cultured for 24 h. Resazurin (10% v/v) was added and the plate was kept in the incubator for 1 h. Resazurin (blue, nonfluorescent) is reduced by live cells to resorufin (pink, fluorescent). The fluorescence intensity of resorufin was then measured by a plate reader. For two-photon luminescence imaging, cells were fixed in 4% paraformaldehyde and stained with Hoescht 33342 (2 μg mL^{-1} in PBS) 30 min prior to imaging.

2.6. Raman Mapping. After particle incubation the cells were fixed with a 4% paraformaldehyde solution and rinsed with water to remove any remaining salt. The coverslips were removed from the 6-well plate and mounted onto glass slides following the protocol for the ProLong Gold Antifade Reagent. After curing for 24 h, the edges of the coverslip were sealed with clear nail polish to extend the sample life. Raman mapping was performed on the Renishaw inVia Raman microscope. Cells were located under brightfield illumination with a 40× objective. Spectra were collected with the grating centered at 1100 cm^{-1} (~600 cm^{-1} bandwidth) during a 5 s data acquisition. The Raman image maps were created by collecting spectra at multiple points on a grid with 2 μm spacing over the 2D region of a cell. The baseline-subtracted intensity from the DTDC peak between 1120 and 1150 cm^{-1} was integrated and then displayed over the grid using a color scale to depict the intensity variation across the area.

2.7. Photodynamic Therapy. After particle incubation, the cells were kept in PBS to prevent any optical interference from the phenol red in the cell culture medium. A region of cells was focused on using a 40× phase contrast objective and then irradiated with light from the mercury arc lamp after passing through a DAPI filter (377/50 nm). The measured power density was 4.4 W/cm^2. After treatment, the PBS was replaced with growth medium, and cells were cultured for 4 h prior to viability staining. Cell viability was assessed by incubating cells for 5 min in a solution of PBS containing 1 μg mL^{-1} FDA for live cells (green) and 50 μg mL^{-1} PI for dead cells (red) and imaging on a fluorescence microscope.

2.8. Data Analysis. Smoothing and baseline subtraction of Raman spectra were performed in MATLAB R2012a. Spectra were smoothed using the "smooth" function with parameters: span = 15, method = "sgolay", degree = 2. The baseline was removed using a numerical algorithm developed in our laboratory, which uses a moving window to locally determine the background fluorescence. Unprocessed versions of the Raman spectra presented in the text can be found in the Supporting Information. Mathematica 8.0.4 was used to integrate the area under the curve for fluorescence spectra of PpIX. Scale bars were added to images using ImageJ 1.46j. All graphs were created in Microsoft Excel for Mac Version 14.2.3.

3. RESULTS AND DISCUSSION

3.1. Nanoparticle Synthesis and Characterization. Scheme 1 presents a visual overview of the steps required to prepare the theranostic nanoplatform. The Raman-labeled gold nanostars (AuNS) were prepared using a similar procedure described in our previous report.[6] PEGylated AuNS were allowed to stir overnight in a solution containing 0.2 μM of the dye DTDC. The sulfur groups of the thiacarbocyanine dye aid in adsorption to the gold surface.[55] Figure 1 shows the SERRS spectrum of the unwashed AuNS-DTDC particle solution before silica coating (solid line), indicating binding of the dye at or near the particle surface. After washing there was little to no change in the intensity of the SERRS spectrum. The decrease in SERRS intensity after silica coating is likely due to displacement of any DTDC that was not bound directly to the particle surface by the condensation of silica onto the PEG layer. Figure 2A shows the absorption spectra of PpIX and DTDC, indicating that excitation at 633 nm does not activate PpIX, and that this excitation is resonant with DTDC, thus producing SERRS.

We coated the PEGylated, labeled AuNS with silica using a method described previously by Fernández-López et al.[54] Adding PEG to the AuNS enhances particle stability in ethanol so that a modified Stöber method can be used to form the silica shell.[56] It is believed that PEG facilitates the condensation of silica through hydrogen binding of PEG ether oxygens and silanol groups.[54] As seen in Figure 2B, there is a red shift in the extinction spectrum of the AuNS after silica coating, caused by an increase in the local refractive index around the particles.[57] PpIX loading of the silica shell was achieved by adding 1 μM of the photosensitizer to the reaction mixture prior to initiation of silica condensation. The drug was sequestered in the pores of the silica matrix, and fluorescence emission of PpIX was

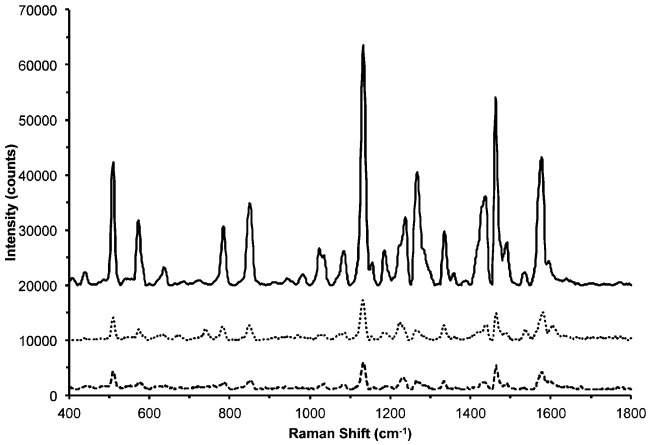

Figure 1. SERRS spectra of AuNS-DTDC solution (solid, top), AuNS-DTDC@SiO_2-PpIX-TAT solution (dotted, middle), and a point collection from a cell that had been incubated with AuNS-DTDC@SiO_2-PpIX-TAT (dashed, bottom). All spectra were acquired at 633 nm excitation (8 mW) with a 10 s integration time. The solution spectra were recorded using a 10× objective with the particles suspended in water, while the intracellular Raman spectrum was recorded with a 40× objective. Spectra are baseline-subtracted and offset for clarity.

observed from the synthesized particles after being washed (Figure 2B). A calibration curve (Figure S1) was established using the fluorescence emission of PpIX under 415 nm excitation and it was estimated that 0.37 ± 0.03 μM of the initial 1 μM PpIX was encapsulated on the AuNS. The fluorescence intensity of PpIX remaining in the supernatant after the silica coating was used to make this estimation. When using the fluorescence intensity from the particle solution itself, a loaded PpIX concentration of 0.18 ± 0.03 μM is determined. This discrepancy can largely be attributed to the inner filter effects of the nanostars, which have an optical density around 0.65 in the excitation band for PpIX and an average optical density of about 0.8 in the PpIX emission band. It is also possible that there are quenching and enhancing effects on the PpIX caused by the gold nanostars; however, a more in-depth discussion of this topic is beyond the scope of this paper.

The particle samples were also tested for any PpIX leaching due to plasmonic heating of the nanostars. A HeNe laser (633 nm) was chosen due to the close matching of the excitation wavelength with the maximum absorption of the nanostars. Aliquots of 100 μL of AuNS-DTDC@SiO_2-PpIX or AuNS-DTDC@SiO_2-PpIX-TAT were placed into a 96-well plate and irradiated with an 8 mW 633 nm laser for various amounts of time. The samples were spun down at 5k rcf, and PpIX fluorescence was measured from the supernatant. It is seen that after 15 min of irradiation, less than 25% of the PpIX has been leached from the nanoparticles (Figure S2). The TAT-coated particles also show a slightly lower rate of PpIX release, possibly due to partial blocking of the silica pores on the outer surface. It is worthy to note that when the delivered light flux is equal to that which is used for PDT (at 1.5 min irradiation time), only ~10% of the loaded PpIX had escaped from the silica shell.

TEM was used to characterize the particle size and morphology. Figure 3 shows that addition of PpIX did not impact the formation of complete silica shells on the AuNS. The hydrodynamic size of the AuNS-DTDC@SiO_2−PpIX was measured to be 123 ± 34 nm by nanoparticle tracking analysis (Figure S3). The final particle modification step was conjugation with the TAT peptide. Electrostatic interaction between the negatively charged silica-coated particles and the

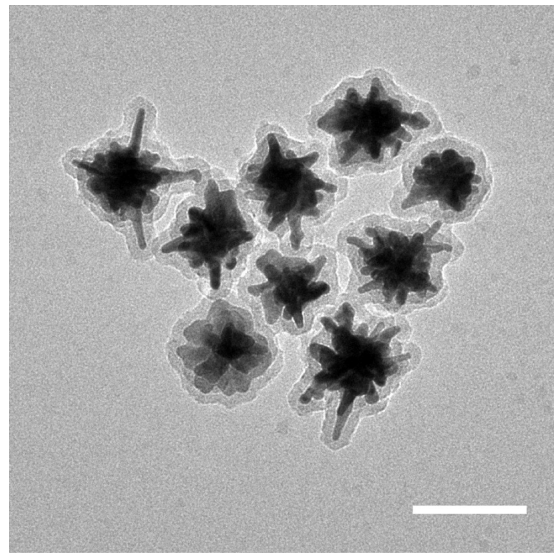

Figure 3. TEM micrograph of the silica coated AuNS. The scale bar is 100 nm.

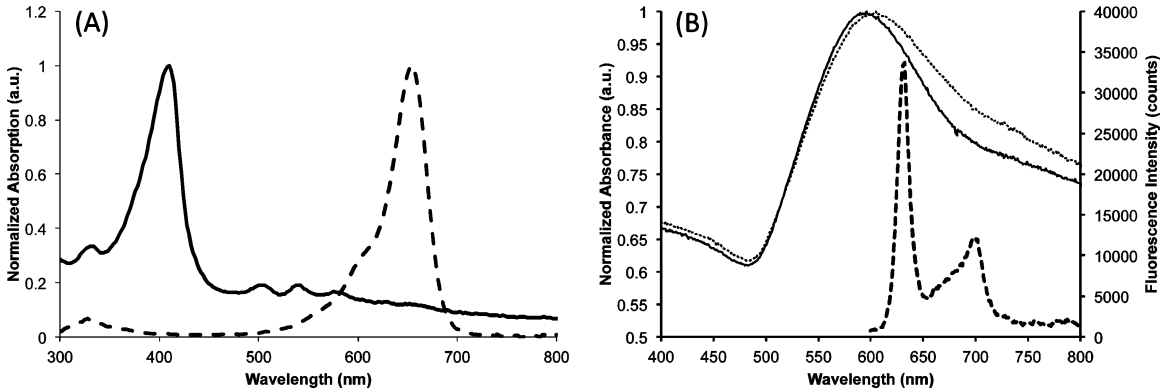

Figure 2. (A) Absorption spectra of free PpIX (solid) and DTDC (dashed) in ethanol. (B) Absorption spectra of the AuNS-DTDC before (solid, left axis) and after (dotted, left axis) silica coating (particles dispersed in water) and fluorescence emission from the AuNS-DTDC@SiO_2-PpIX-TAT (dispersed in ethanol) under 415 nm excitation (dashed, right axis).

positively charged TAT peptide induce an effective attachment method. This attachment is confirmed by the dramatic increase in intracellular particle accumulation observed for the TAT functionalized particles by two-photon luminescence imaging (Figure S4).

Although silica nanoparticles are generally considered to be nontoxic, the pronounced increase in particle uptake caused by the TAT peptide warranted the use of a cytotoxicity assay to measure the impact of this dense particle loading. Cells in a 96-well plate were incubated with various particle samples at a concentration of 0.1 nM for 1 h, washed in PBS, and then cultured for 24 h. After this time period, a resazurin assay was used to assess the cytotoxicity of each particle sample (Figure 4). Each data set is the average fluorescence intensity from a

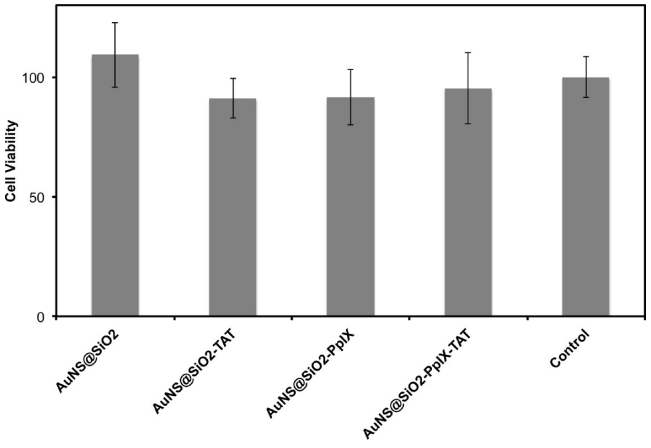

Figure 4. Cell viability after a 1 h incubation with various particle samples at a concentration of 0.1 nM. The error bars are ± one standard deviation of eight measurements.

column on the 96-well plate (eight measurements). It can be seen from the figure that there is no statistically significant difference in cell viability for any of the particle-incubated samples compared to the control sample.

3.2. Raman Mapping. Raman images were created by taking a 5 s spectral acquisition centered at 1100 cm^{-1} (~600 cm^{-1} bandwidth) at each point on a grid with 2 μm spacing over the 2D area of a cell. The integrated DTDC peak intensity between 1120 and 1150 cm^{-1} was displayed over the area using a color map to depict intensity variation. This peak was chosen because it showed the highest signal intensity. Representative Raman images are displayed in Figure 5. The color scale was kept constant across all of the images to allow for a fair comparison between them. In contrast, little to no Raman signal was detected from cells incubated with AuNP-DTDC@SiO_2-PpIX without TAT (Figure S5), which is in good agreement with the TPL imaging results (Figure S4).

3.3. Photodynamic Therapy. The efficacy of our theranostic construct was demonstrated using cell viability staining after exposing nanoparticle-incubated cells to UV light. The treatment group was incubated with AuNS-DTDC@SiO_2-PpIX-TAT for 1 h while the control group was incubated with AuNS-DTDC@SiO_2-TAT for 1 h (particle concentration of 0.1 nM). The cells were washed 3× in PBS and then exposed to light for 30 s from a mercury arc lamp after passing through a DAPI filter (377/50 nm). A 40× objective was used to focus the light onto the cell sample, with a measured power density of 4.4 W cm^{-2}. After treatment, cells were cultured for 4 h in complete growth medium prior to viability staining. Results of the viability staining are shown in Figure 6. Cell death due to PDT is highly evident in Figure 6 (left). There appears to be some cell detachment in the control group (Figure 6, right) due to heating of the nanoparticles, but the result is not as dramatic as that seen with the PpIX-loaded particles. The mechanism of photocytotoxicity is ascribed to the $^1O_2$ generated by PpIX when excited by the broadband light within its absorption band. This $^1O_2$ can diffuse out of the porous silica matrix and travel on the order of tens of nanometers to affect cellular components. While the excitation light did heat the particles enough to cause some cell detachment, very few of the cells were actually ablated (red-stained cells, Figure 6, right). The effect of using PpIX-loaded particles without TAT was also tested. Light exposure after a 1 h incubation with 0.1 nM AuNS-DTDC@SiO_2-PpIX did not produce any observable effect (Figure S6).

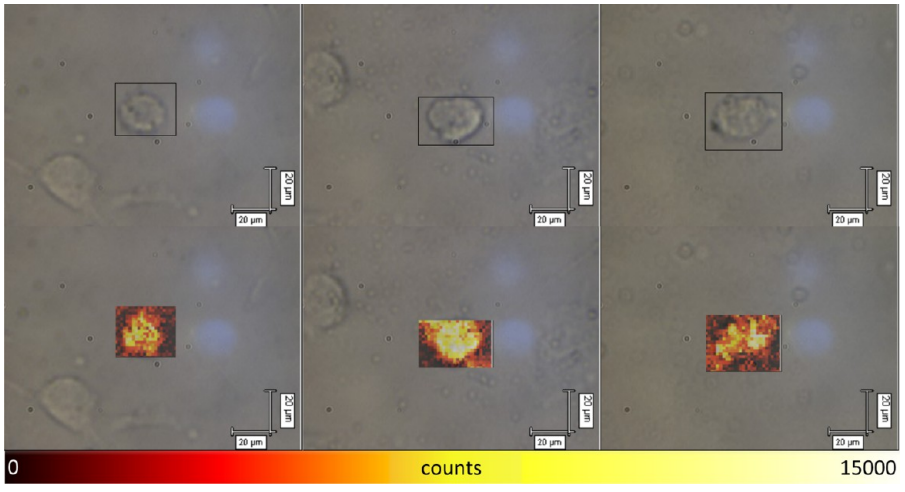

Figure 5. Three representative Raman images of cells incubated with AuNS-DTDC@SiO_2-PpIX-TAT, collected with 633 nm excitation (8 mW). The top row shows the brightfield image and selected area, while the bottom row displays the calculated Raman image. The calculated intensity values came from the integrated peak intensity of the baseline-subtracted DTDC peak between 1120 and 1150 cm^{-1}. The intensity scale is shown beneath the images and was kept constant across all acquisitions.

dx.doi.org/10.1021/mp300634b | *Mol. Pharmaceutics* 2013, 10, 2291−2298

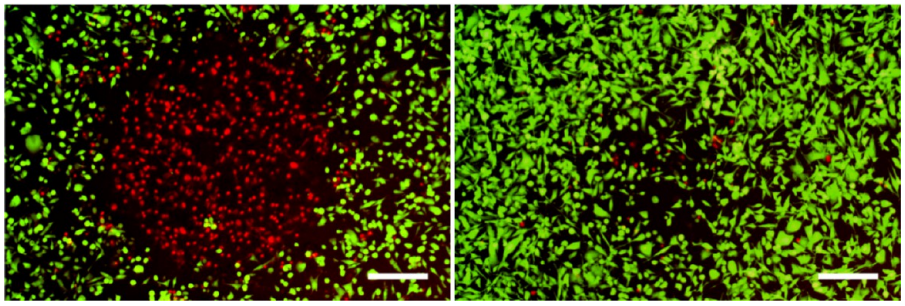

Figure 6. Viability staining of cells incubated with AuNS-DTDC@SiO_2-PpIX-TAT (left) and AuNS-DTDC@SiO_2-TAT (right) after 30 s of light irradiation. Live cells are stained green, and dead cells are stained red. Scale bars are 250 μm.

4. CONCLUSIONS

In summary, we present the first application of a theranostic, combined Raman imaging and photosensitizer nanoconstruct. The use of the cell-penetrating peptide, TAT, greatly increases particle uptake by the cells, enhancing the efficacy of our construct. Raman imaging and photosensitization were demonstrated on BT-549 breast cancer cells. When the same conditions were used for particles that were not functionalized with TAT, little to no Raman signal could be detected from the cells, and no photosensitization was observed after light exposure. The particles exhibited no cytotoxic effect under dark conditions. Future work will involve the use of various targeting ligands and multiple Raman probes to investigate the specificity and multiplexing capability of our theranostic construct. The use of other drugs, not only photosensitizers, is currently under investigation.

■ ASSOCIATED CONTENT

Ⓢ Supporting Information

Supplementary figures S1−S9. This material is available free of charge via the Internet at http://pubs.acs.org.

■ AUTHOR INFORMATION

Corresponding Author

*Duke University, 136 Hudson Hall, Box 90281, Durham, North Carolina 27708, United States. Phone: 919-660-8520. Fax: 919-613-9145. E-mail: tuan.vodinh@duke.edu.

Notes

The authors declare no competing financial interest.

■ ACKNOWLEDGMENTS

This work was sponsored by the Duke University Faculty Research Funds. A.M.F. is supported by an NIH training grant (T32 EB001040).

■ REFERENCES

(1) Minelli, C.; Lowe, S. B.; Stevens, M. M. Engineering Nanocomposite Materials for Cancer Therapy. *Small* **2010**, *6* (21), 2336−2357.

(2) Janib, S. M.; Moses, A. S.; MacKay, J. A. Imaging and drug delivery using theranostic nanoparticles. *Adv. Drug Delivery Rev.* **2010**, *62* (11), 1052−1063.

(3) Lammers, T.; Kiessling, F.; Hennink, W. E.; Storm, G. Nanotheranostics and Image-Guided Drug Delivery: Current Concepts and Future Directions. *Mol. Pharmaceutics* **2010**, *7* (6), 1899−1912.

(4) Xie, J.; Lee, S.; Chen, X. Nanoparticle-based theranostic agents. *Adv. Drug Delivery Rev.* **2010**, *62* (11), 1064−1079.

(5) Mura, S.; Couvreur, P. Nanotheranostics for personalized medicine. *Adv. Drug Delivery Rev.* **2012**, *64* (13), 1394−416.

(6) Fales, A. M.; Yuan, H.; Vo-Dinh, T. Silica-Coated Gold Nanostars for Combined Surface-Enhanced Raman Scattering (SERS) Detection and Singlet-Oxygen Generation: A Potential Nanoplatform for Theranostics. *Langmuir* **2011**, *27* (19), 12186−12190.

(7) Yuan, H.; Fales, A. M.; Vo-Dinh, T. TAT Peptide-Functionalized Gold Nanostars: Enhanced Intracellular Delivery and Efficient NIR Photothermal Therapy Using Ultralow Irradiance. *J. Am. Chem. Soc.* **2012**, *134* (28), 11358−11361.

(8) Yuan, H.; Khoury, C. G.; Wilson, C. M.; Grant, G. A.; Bennett, A. J.; Vo-Dinh, T. In vivo particle tracking and photothermal ablation using plasmon-resonant gold nanostars. *Nanomedicine* **2012**, *8* (8), 1355−63.

(9) Yuan, H.; Khoury, C. G.; Hwang, H.; Wilson, C. M.; Grant, G. A.; Vo-Dinh, T. Gold nanostars: surfactant-free synthesis, 3D modelling, and two-photon photoluminescence imaging. *Nanotechnology* **2012**, *23* (7), 075102.

(10) Vo-Dinh, T.; Hiromoto, M. Y. K.; Begun, G. M.; Moody, R. L. Surface-enhanced Raman spectrometry for trace organic analysis. *Anal. Chem.* **1984**, *56* (9), 1667−1670.

(11) Vo-Dinh, T.; Meier, M.; Wokaun, A. Surface-enhanced Raman spectrometry with silver particles on stochastic-post substrates. *Anal. Chim. Acta* **1986**, *181* (0), 139−148.

(12) Vo-Dinh, T. Surface-enhanced Raman spectroscopy using metallic nanostructures. *Trends Anal. Chem.* **1998**, *17* (8−9), 557−582.

(13) Vo-Dinh, T.; Dhawan, A.; Norton, S. J.; Khoury, C. G.; Wang, H.-N.; Misra, V.; Gerhold, M. D. Plasmonic Nanoparticles and Nanowires: Design, Fabrication and Application in Sensing†. *J. Phys. Chem. C* **2010**, *114* (16), 7480−7488.

(14) Bálint, Š.; Rao, S.; Marro, M.; Miškovský, P.; Petrov, D. Monitoring of local pH in photodynamic therapy-treated live cancer cells using surface-enhanced Raman scattering probes. *J. Raman Spectrosc.* **2011**, *42* (6), 1215−1221.

(15) Kircher, M. F.; de la Zerda, A.; Jokerst, J. V.; Zavaleta, C. L.; Kempen, P. J.; Mittra, E.; Pitter, K.; Huang, R.; Campos, C.; Habte, F.; Sinclair, R.; Brennan, C. W.; Mellinghoff, I. K.; Holland, E. C.; Gambhir, S. S. A brain tumor molecular imaging strategy using a new triple-modality MRI-photoacoustic-Raman nanoparticle. *Nat. Med.* **2012**, *18* (5), 829−834.

(16) Alvarez-Puebla, R. A.; Liz-Marzán, L. M. SERS-Based Diagnosis and Biodetection. *Small* **2010**, *6* (5), 604−610.

(17) Kneipp, J.; Kneipp, H.; Wittig, B.; Kneipp, K. Following the Dynamics of pH in Endosomes of Live Cells with SERS Nanosensors. *J. Phys. Chem. C* **2010**, *114* (16), 7421−7426.

(18) Kneipp, J.; Kneipp, H.; Rice, W. L.; Kneipp, K. Optical Probes for Biological Applications Based on Surface-Enhanced Raman Scattering from Indocyanine Green on Gold Nanoparticles. *Anal. Chem.* **2005**, *77* (8), 2381−2385.

(19) Kneipp, J.; Kneipp, H.; Rajadurai, A.; Redmond, R. W.; Kneipp, K. Optical probing and imaging of live cells using SERS labels. *J. Raman Spectrosc.* **2009**, *40* (1), 1−5.

(20) Qian, X. M.; Nie, S. M. Single-molecule and single-nanoparticle SERS: from fundamental mechanisms to biomedical applications. *Chem. Soc. Rev.* **2008**, *37* (5), 912−920.
(21) Faulds, K.; Smith, W. E.; Graham, D. Evaluation of Surface-Enhanced Resonance Raman Scattering for Quantitative DNA Analysis. *Anal. Chem.* **2003**, *76* (2), 412−417.
(22) Rodriguez-Lorenzo, L.; Krpetic, Z.; Barbosa, S.; Alvarez-Puebla, R. A.; Liz-Marzan, L. M.; Prior, I. A.; Brust, M. Intracellular mapping with SERS-encoded gold nanostars. *Integr. Biol.* **2011**, *3* (9), 922−926.
(23) Küstner, B.; Gellner, M.; Schütz, M.; Schöppler, F.; Marx, A.; Ströbel, P.; Adam, P.; Schmuck, C.; Schlücker, S. SERS Labels for Red Laser Excitation: Silica-Encapsulated SAMs on Tunable Gold/Silver Nanoshells. *Angew. Chem., Int. Ed.* **2009**, *48* (11), 1950−1953.
(24) Cao, Y. C.; Jin, R.; Nam, J.-M.; Thaxton, C. S.; Mirkin, C. A. Raman Dye-Labeled Nanoparticle Probes for Proteins. *J. Am. Chem. Soc.* **2003**, *125* (48), 14676−14677.
(25) Wang, G.; Park, H.-Y.; Lipert, R. J.; Porter, M. D. Mixed Monolayers on Gold Nanoparticle Labels for Multiplexed Surface-Enhanced Raman Scattering Based Immunoassays. *Anal. Chem.* **2009**, *81* (23), 9643−9650.
(26) Gregas, M. K.; Yan, F.; Scaffidi, J.; Wang, H.-N.; Vo-Dinh, T. Characterization of nanoprobe uptake in single cells: spatial and temporal tracking via SERS labeling and modulation of surface charge. *Nanomedicine: NBM* **2011**, *7* (1), 115−122.
(27) Gregas, M. K.; Scaffidi, J. P.; Lauly, B.; Vo-Dinh, T. Surface-Enhanced Raman Scattering Detection and Tracking of Nanoprobes: Enhanced Uptake and Nuclear Targeting in Single Cells. *Appl. Spectrosc.* **2010**, *64* (8), 858−866.
(28) Zavaleta, C. L.; Smith, B. R.; Walton, I.; Doering, W.; Davis, G.; Shojaei, B.; Natan, M. J.; Gambhir, S. S. Multiplexed imaging of surface enhanced Raman scattering nanotags in living mice using noninvasive Raman spectroscopy. *Proc. Natl. Acad. Sci. U.S.A.* **2009**, *106* (32), 13511−13516.
(29) Keren, S.; Zavaleta, C.; Cheng, Z.; de la Zerda, A.; Gheysens, O.; Gambhir, S. S. Noninvasive molecular imaging of small living subjects using Raman spectroscopy. *Proc. Natl. Acad. Sci. U.S.A.* **2008**, *105* (15), 5844−5849.
(30) Kim, J.-H.; Kim, J.-S.; Choi, H.; Lee, S.-M.; Jun, B.-H.; Yu, K.-N.; Kuk, E.; Kim, Y.-K.; Jeong, D. H.; Cho, M.-H.; Lee, Y.-S. Nanoparticle Probes with Surface Enhanced Raman Spectroscopic Tags for Cellular Cancer Targeting. *Anal. Chem.* **2006**, *78* (19), 6967−6973.
(31) Yuan, H.; Liu, Y.; Fales, A. M.; Li, Y. L.; Liu, J.; Vo-Dinh, T. Quantitative Surface-Enhanced Resonant Raman Scattering Multiplexing of Biocompatible Gold Nanostars for in Vitro and ex Vivo Detection. *Anal. Chem.* **2012**, *85* (1), 208−212.
(32) Lam, M.; Oleinick, N. L.; Nieminen, A.-L. Photodynamic Therapy-induced Apoptosis in Epidermoid Carcinoma Cells. *J. Biol. Chem.* **2001**, *276* (50), 47379−47386.
(33) Tang, W.; Xu, H.; Kopelman, R.; Philbert, M. A. Photodynamic Characterization and In Vitro Application of Methylene Blue-containing Nanoparticle Platforms. *Photochem. Photobiol.* **2005**, *81* (2), 242−249.
(34) Rossi, L. M.; Silva, P. R.; Vono, L. L. R.; Fernandes, A. U.; Tada, D. B.; Baptista, M. c. S. Protoporphyrin IX Nanoparticle Carrier: Preparation, Optical Properties, and Singlet Oxygen Generation. *Langmuir* **2008**, *24* (21), 12534−12538.
(35) Lee, S. J.; Koo, H.; Lee, D.-E.; Min, S.; Lee, S.; Chen, X.; Choi, Y.; Leary, J. F.; Park, K.; Jeong, S. Y.; Kwon, I. C.; Kim, K.; Choi, K. Tumor-homing photosensitizer-conjugated glycol chitosan nanoparticles for synchronous photodynamic imaging and therapy based on cellular on/off system. *Biomaterials* **2011**, *32* (16), 4021−4029.
(36) Bechet, D.; Couleaud, P.; Frochot, C.; Viriot, M.-L.; Guillemin, F.; Barberi-Heyob, M. Nanoparticles as vehicles for delivery of photodynamic therapy agents. *Trends Biotechnol.* **2008**, *26* (11), 612−621.
(37) Roy, I.; Ohulchanskyy, T. Y.; Pudavar, H. E.; Bergey, E. J.; Oseroff, A. R.; Morgan, J.; Dougherty, T. J.; Prasad, P. N. Ceramic-Based Nanoparticles Entrapping Water-Insoluble Photosensitizing Anticancer Drugs: A Novel Drug−Carrier System for Photodynamic Therapy. *J. Am. Chem. Soc.* **2003**, *125* (26), 7860−7865.
(38) Ohulchanskyy, T. Y.; Roy, I.; Goswami, L. N.; Chen, Y.; Bergey, E. J.; Pandey, R. K.; Oseroff, A. R.; Prasad, P. N. Organically Modified Silica Nanoparticles with Covalently Incorporated Photosensitizer for Photodynamic Therapy of Cancer. *Nano Lett.* **2007**, *7* (9), 2835−2842.
(39) Kim, S.; Ohulchanskyy, T. Y.; Pudavar, H. E.; Pandey, R. K.; Prasad, P. N. Organically Modified Silica Nanoparticles Co-encapsulating Photosensitizing Drug and Aggregation-Enhanced Two-Photon Absorbing Fluorescent Dye Aggregates for Two-Photon Photodynamic Therapy. *J. Am. Chem. Soc.* **2007**, *129* (9), 2669−2675.
(40) Yan, F.; Kopelman, R. The Embedding of Meta-tetra-(Hydroxyphenyl)-Chlorin into Silica Nanoparticle Platforms for Photodynamic Therapy and Their Singlet Oxygen Production and pH-dependent Optical Properties. *Photochem. Photobiol.* **2003**, *78* (6), 587−591.
(41) Lu, J.; Liong, M.; Zink, J. I.; Tamanoi, F. Mesoporous Silica Nanoparticles as a Delivery System for Hydrophobic Anticancer Drugs. *Small* **2007**, *3* (8), 1341−1346.
(42) Zhao, T.; Wu, H.; Yao, S. Q.; Xu, Q.-H.; Xu, G. Q. Nanocomposites Containing Gold Nanorods and Porphyrin-Doped Mesoporous Silica with Dual Capability of Two-Photon Imaging and Photosensitization. *Langmuir* **2010**, *26* (18), 14937−14942.
(43) Qian, H. S.; Guo, H. C.; Ho, P. C.-L.; Mahendran, R.; Zhang, Y. Mesoporous-Silica-Coated Up-Conversion Fluorescent Nanoparticles for Photodynamic Therapy. *Small* **2009**, *5* (20), 2285−2290.
(44) Tada, D. B.; Vono, L. L. R.; Duarte, E. L.; Itri, R.; Kiyohara, P. K.; Baptista, M. S.; Rossi, L. M. Methylene Blue-Containing Silica-Coated Magnetic Particles: A Potential Magnetic Carrier for Photodynamic Therapy. *Langmuir* **2007**, *23* (15), 8194−8199.
(45) Zhang, Z.; Wang, L.; Wang, J.; Jiang, X.; Li, X.; Hu, Z.; Ji, Y.; Wu, X.; Chen, C. Mesoporous Silica-Coated Gold Nanorods as a Light-Mediated Multifunctional Theranostic Platform for Cancer Treatment. *Adv. Mater.* **2012**, *24* (11), 1418−1423.
(46) Yuan, H.; Fales, A. M.; Khoury, C. G.; Liu, J.; Vo-Dinh, T. Spectral characterization and intracellular detection of Surface-Enhanced Raman Scattering (SERS)-encoded plasmonic gold nanostars. *J. Raman Spectrosc.* **2013**, *44* (2), 234−239.
(47) de la Fuente, J. M.; Berry, C. C. Tat Peptide as an Efficient Molecule To Translocate Gold Nanoparticles into the Cell Nucleus. *Bioconjugate Chem.* **2005**, *16* (5), 1176−1180.
(48) Santra, S.; Yang, H.; Dutta, D.; Stanley, J. T.; Holloway, P. H.; Tan, W.; Moudgil, B. M.; Mericle, R. A. TAT conjugated, FITC doped silica nanoparticles for bioimaging applications. *Chem. Commun.* **2004**, *024*, 2810−2811.
(49) Torchilin, V. P. Tat peptide-mediated intracellular delivery of pharmaceutical nanocarriers. *Adv. Drug Delivery Rev.* **2008**, *60* (4−5), 548−558.
(50) Pan, L.; He, Q.; Liu, J.; Chen, Y.; Ma, M.; Zhang, L.; Shi, J. Nuclear-Targeted Drug Delivery of TAT Peptide-Conjugated Monodisperse Mesoporous Silica Nanoparticles. *J. Am. Chem. Soc.* **2012**, *134* (13), 5722−5725.
(51) Sebbage, V. Cell-penetrating peptides and their therapeutic applications. *Biosci. Horizons* **2009**, *2* (1), 64−72.
(52) Ruan, G.; Agrawal, A.; Marcus, A. I.; Nie, S. Imaging and Tracking of Tat Peptide-Conjugated Quantum Dots in Living Cells: New Insights into Nanoparticle Uptake, Intracellular Transport, and Vesicle Shedding. *J. Am. Chem. Soc.* **2007**, *129* (47), 14759−14766.
(53) Scaffidi, J. P.; Gregas, M. K.; Lauly, B.; Zhang, Y.; Vo-Dinh, T. Activity of Psoralen-Functionalized Nanoscintillators against Cancer Cells upon X-ray Excitation. *ACS Nano* **2011**, *5* (6), 4679−4687.
(54) Fernández-López, C.; Mateo-Mateo, C.; Álvarez-Puebla, R. n. A.; Pérez-Juste, J.; Pastoriza-Santos, I.; Liz-Marzán, L. M. Highly Controlled Silica Coating of PEG-Capped Metal Nanoparticles and Preparation of SERS-Encoded Particles. *Langmuir* **2009**, *25* (24), 13894−13899.
(55) Vujačić, A.; Vasić, V.; Dramićanin, M.; Sovilj, S. P.; Bibić, N.; Hranisavljevic, J.; Wiederrecht, G. P. Kinetics of J-Aggregate

Formation on the Surface of Au Nanoparticle Colloids. *J. Phys. Chem. C* **2012**, *116* (7), 4655−4661.
(56) Stöber, W.; Fink, A.; Bohn, E. Controlled growth of monodisperse silica spheres in the micron size range. *J. Colloid Interface Sci.* **1968**, *26* (1), 62−69.
(57) Liz-Marzán, L. M.; Giersig, M.; Mulvaney, P. Synthesis of Nanosized Gold−Silica Core−Shell Particles. *Langmuir* **1996**, *12* (18), 4329−4335.